Electron paramagnetic resonance investigation of polycrystalline $CaCu_3Ti_4O_{12}$

2003 J. Phys.: Condens. Matter 15 7365

(http://iopscience.iop.org/0953-8984/15/43/018)

INSTITUTE OF PHYSICS PUBLISHING JOURNAL OF PHYSICS: CONDENSED MATTER

J. Phys.: Condens. Matter **15** (2003) 7365–7374 PII: S0953-8984(03)65181-7

Electron paramagnetic resonance investigation of polycrystalline $CaCu_3Ti_4O_{12}$

Maria Cristina Mozzati[1,3], Carlo Bruno Azzoni[1], Doretta Capsoni[2], Marcella Bini[2] and Vincenzo Massarotti[2]

[1] INFM-Dipartimento di Fisica 'Alessandro Volta', Università di Pavia, via Bassi 6, I-27100 Pavia, Italy
[2] Dipartimento di Chimica Fisica 'Mario Rolla', Università di Pavia and IENI-CNR, Sezione di Pavia, viale Taramelli 16, I-27100 Pavia, Italy

E-mail: mozzati@fisicavolta.unipv.it

Received 18 June 2003, in final form 16 September 2003
Published 17 October 2003
Online at stacks.iop.org/JPhysCM/15/7365

Abstract

Electron paramagnetic resonance (EPR) measurements on pure polycrystalline $CaCu_3Ti_4O_{12}$ have been performed and are discussed within a crystal-field approach. A symmetric signal centred at $g = 2.15$ is observed for $T > 25$ K, with no evidence of hyperfine structure. At this temperature an antiferromagnetic transition is observed as confirmed by static magnetization data. Cu defective and 2% doped (V, Cr, Mn, La) samples were also prepared and considered, mainly to understand the nature of the observed paramagnetic centre. Substitutions in the octahedral sites, causing variations of the configuration in CuO_4–TiO_6–CuO_4 complexes, change the magnetic and EPR features. To justify the EPR response a strong copper-hole delocalization is suggested.

1. Introduction

The perovskite-type $CaCu_3Ti_4O_{12}$ has recently received a great deal of interest for the so-called 'giant-dielectric phenomenon'. Such material displays unusual dielectric properties [1–3], very important for high performance capacitors, attributed to a grain boundary barrier layer capacitance related to the ceramic microstructure (average grain size and pellet density) and processing conditions (oxygen partial pressure, sintering temperature and cooling rate) [4]. However the final explanation of the very high permittivity ($>10^4$ and nearly temperature independent over the 100–600 K range) remains undefined and further investigations are required.

[3] Author to whom any correspondence should be addressed.

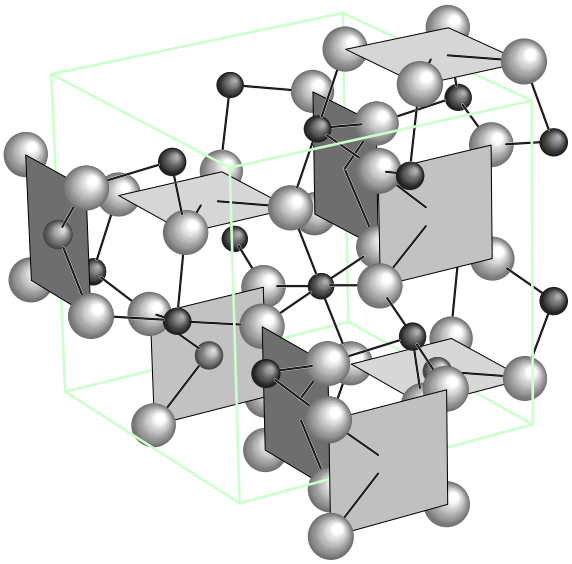

Figure 1. $CaCu_3Ti_4O_{12}$ structure: the square-planar CuO_4 groups and the Cu–Ti links *via* oxygen ions are shown (oxygen: light grey sphere, titanium: black sphere, copper: dark grey sphere; Ca ions are omitted for clarity).

(This figure is in colour only in the electronic version)

A high degree of twinning, as verified by x-ray and neutron powder diffraction [2, 5, 6] and confirmed by single crystals measurements [2], suggested the presence of small domains that can explain the peculiar dielectric properties [2]. The cubic cell is body centred ($Im\bar{3}$, $a = 0.7391$ nm, $Z = 2$) with inversion symmetry so the possibility of a net spontaneous polarization is precluded.

With regard to the magnetic properties, $CaCu_3Ti_4O_{12}$ shows an antiferromagnetic (AF) transition at ∼25 K [7], explained in terms of a double primitive cell in which each Cu–Cu nearest neighbour pair has antiparallel spins [8]. As regards the electron paramagnetic resonance (EPR) features of this compound, to our knowledge only one study has been reported in the literature, in 1977 [9].

Cu defective and substituted samples showed dielectric properties appreciably modified with respect to those of the pure sample [2]. It is also reasonable to expect that low substitutions of transition ions, such as Mn, Cr and V in the octahedral Ti site and of La in the Ca site, can yield changes of the magnetic features and, consequently, of the EPR response. In this work we report on EPR measurements performed in the temperature range 4–500 K on two pure samples, one of them Cu defective, and on 2% doped (V, Cr, Mn, La) polycrystalline samples of $CaCu_3Ti_4O_{12}$. To explain the electronic structure of the observed paramagnetic centre, the experimental results are discussed within a crystal-field (CF) approach taking into account the structural data. The Ca^{2+} ion is dodecahedrally coordinated with oxygen ions, Cu^{2+} is in a square-planar coordination (as nearest neighbour) and Ti^{4+} coordinates six oxygen ions in a slightly distorted octahedron. The TiO_6 groups are tilted at about 20° with respect to the cell axis [5]. The CuO_4 and TiO_6 units share oxygen ions as shown in figure 1. For each single Cu^{2+} ion, three different perpendicular square-planar oxygen groups can be observed at 0.1961(2), 0.2783(2) and 0.3269(2) nm bond length [5].

2. Experimental details

All the samples were prepared by solid state synthesis from the reagents $TiO_2/CaCO_3/CuO$ and the oxides of the doping elements in appropriate amounts. The mixtures were treated for 84 h at 1273 K in air with four intermediate grindings. A last step of 16 h at 1323 K was performed, after pressing the powders into pellets, to obtain pure $CaCu_3Ti_4O_{12}$ (pure-a) and $Ca_{1-x}A_xCu_3Ti_4O_{12}$ and $CaCu_3Ti_{4-y}B_yO_{12}$ (A = La, $x = 0.02$; B = V, Cr, Mn, $y = 0.08$) doped samples. A second pure sample (pure-b) was prepared using the same thermal cycle but it was gently ground; after that the powder was pressed into pellets and further treated for 12 h at 1323 K.

X-ray powder diffraction (XRPD) measurements were performed using a Bruker D5005 Bragg–Brentano diffractometer equipped with curved graphite monochromator on the diffracted beam. Cu Kα radiation (K$\alpha_1 = 0.154\,056$ nm, K$\alpha_2 = 0.154\,43$ nm) was used. The Rietveld profile refinement [10] was used to obtain structural and profile parameters as well as the amount of each phase (wt%).

EPR measurements were carried out using an X-band (about 9.3 GHz) Bruker spectrometer. A continuous nitrogen flow cryostat, in the temperature range 150–500 K, and an Oxford cryostat with helium continuous flux, in the temperature range 4–150 K, were used. The masses of the samples were a few milligrams. The number of the EPR centres was estimated by comparing the signal areas with that of a paramagnetic standard (Li_2MnO_3) [11] with resonant field and line-width (ΔB) similar to the experimental signals and taking particular care regarding the reproducibility of the samples position in the resonant cavity. For the pure-a sample the signal area agrees with a number of paramagnetic centres with $S = 1/2$ corresponding to the copper amount ($\sim 3 \times 10^{21}$ g^{-1}). Shape and area of the EPR spectra were analysed by numerical methods.

Static magnetization measurements were performed from 300 down to 2 K in a 10^{-2} T magnetic field by means of a SQUID Quantum Design Magnetometer.

3. Results

From XRPD measurements it can be seen that the pure-a sample shows only the diffraction reflections pertinent to the $CaCu_3Ti_4O_{12}$ phase [5]; this is verified also for all the 2% doped samples. In contrast, pure-b shows additional very low peaks due to CuO, whose amount, determined by Rietveld profile refinement, is 0.5(1) wt%. The narrowness of the diffraction lines is comparable in all the samples, confirming a good sintering of the powder and similar values of the crystallite size. A rough estimation of these values, greater than or equal to 300 nm, was made by XRPD profile analysis and full width at half maximum (FWHM) determination. The cell parameter values obtained for V and Cr doped samples are in good agreement with those of pure-a $CaCu_3Ti_4O_{12}$ (0.739 17(1) nm), whereas the other doped samples and pure-b one show comparable a values, ranging from 0.739 23(1) to 0.739 31(1) nm, slightly above that of the pure-a one.

In figure 2 the EPR spectrum of the pure-a sample is shown at different temperatures. Only a symmetric signal centred at $g = 2.15$ is observed for $T > 25$ K. No hyperfine structure is evidenced. The line-shape is Lorentzian with the minimum ΔB value ($\sim$5 mT) at 235 K (figure 3). At about 25 K (T_N), where the AF transition occurs [7], the spectrum splits into two symmetric components. The main one broadens with lower temperature and moves towards low magnetic fields disappearing at about 10 K. This signal behaviour, due to the onset of local magnetic ordering, is well evidenced in figure 4 for the T in the range 14–19 K. The resonant field of the weaker component does not change in all the investigated temperature ranges.

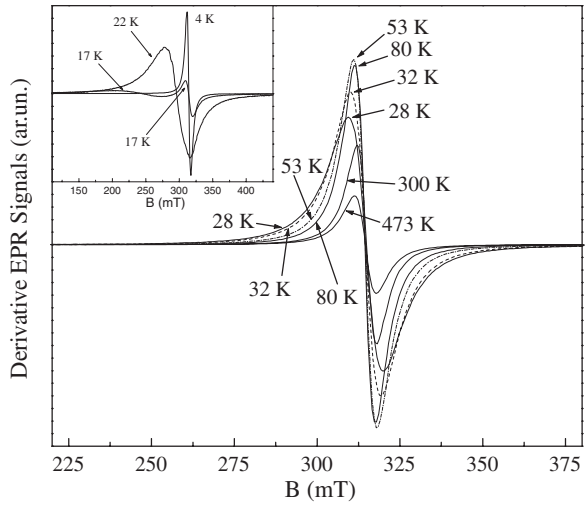

Figure 2. EPR spectra of the pure-a sample for $T > T_N$. The inset shows EPR spectra at 22 and 17 K (amplified by a factor 10) and at 4 K (amplified by a factor 2).

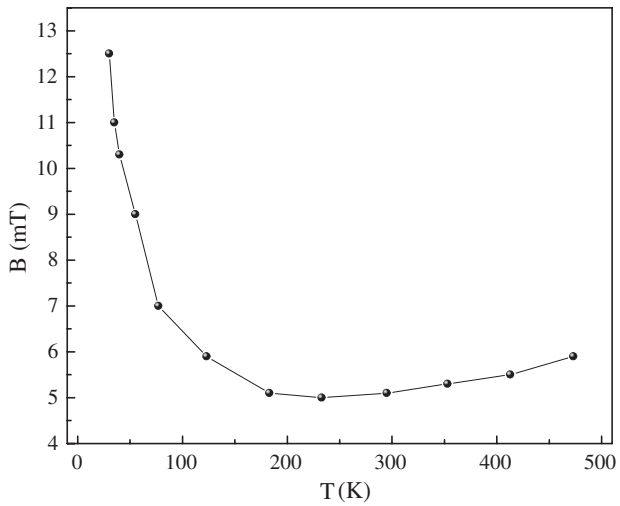

Figure 3. EPR $\Delta B(T)$ behaviour of the pure-a sample for $T > T_N$.

The remaining intensity (area) of this signal component at 4 K (I_4) is about 1/60 of the whole signal intensity (I_{25}) for T just higher than T_N, taking into account the Boltzmann factor. The temperature dependence of the whole signal area up to 4 K is shown in figure 5.

Static magnetization measurements, as shown in figure 6, confirm the T_N value reported in the literature [7] and a spin value $S = 1/2$ from the slope of the $1/\chi$ curve in the paramagnetic region.

The room temperature (RT) EPR signals of the doped samples $Ca_{1-x}A_xCu_3Ti_4O_{12}$ and $CaCu_3Ti_{4-y}B_yO_{12}$ (A = La, $x = 0.02$; B = V, Cr, Mn, $y = 0.08$) are shown in figure 7. The signals of all the samples with substitutions in the octahedral Ti sites can be resolved into two or more components with the same g-factor but different ΔB, as illustrated in figure 8 for the Mn

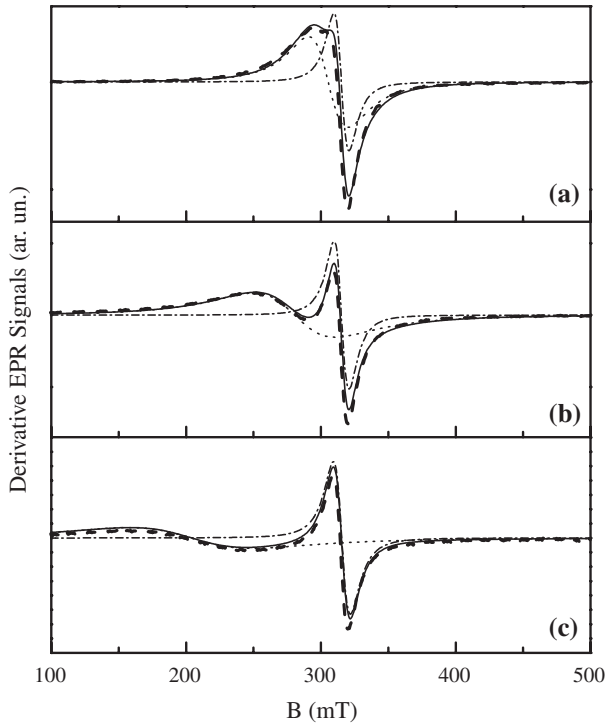

Figure 4. Pure-a sample EPR signal (bold broken curves) at 19 K (a), 18 K (b) and 14 K (c). Dotted and chain curves represent the two symmetric components as obtained by signal simulation (full curves).

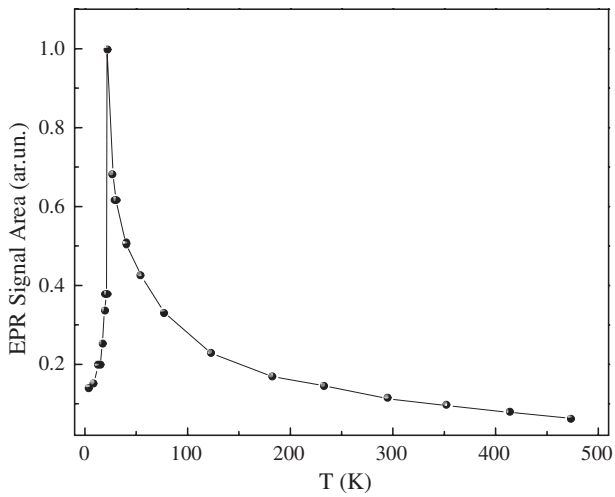

Figure 5. Temperature dependence of the EPR whole signal area of the pure-a sample up to 4 K.

doped sample, selected as an example. For these samples, the signal area abruptly decreases for $T < 25$ K even if the AF transition is less evident with respect to the pure-a sample. The ratio I_4/I_{25} ranges between $1/10$ (Cr doped sample) and $1/30$ (Mn doped sample). The $\Delta B(T)$ behaviour for the Cr doped sample is peculiar because ΔB decreases monotonically

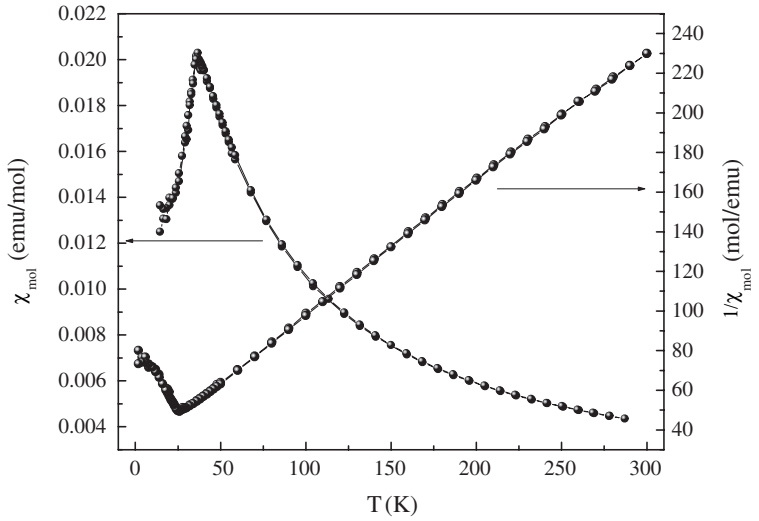

Figure 6. Molar magnetic susceptibility and reciprocal magnetic susceptibility of the pure-a sample at 0.01 T.

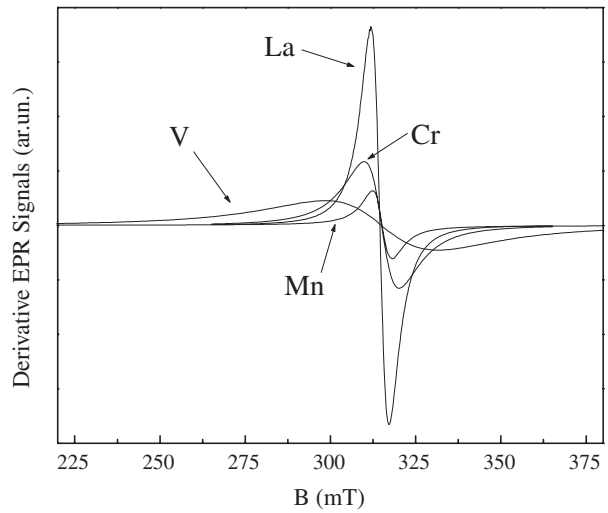

Figure 7. EPR signals at room temperature of La, Cr, V and Mn doped samples. The signal of the V doped sample is multiplied by a factor 5.

with T down to very low temperatures, the other samples showing a minimum ΔB value around 235 K, as the pure-a sample. For the sample with substitution in Ca sites, the signal shape and g-factor do not differ from the signal of the pure-a sample as much as the observed ΔB temperature dependence, T_N and I_4/I_{25} values.

The EPR signal intensity of the pure-b sample, in which the segregation of 0.5% of CuO phase implies the presence of the same number of Cu vacancies in the $CaCu_3Ti_4O_{12}$ structure, is reduced by 50%, at RT, with respect to the pure-a sample. Moreover, $I_4/I_{25} \sim 1/20$ and the paramagnetic signal component for $T < T_N$ (25 K) is well evidenced from the static magnetization measurements.

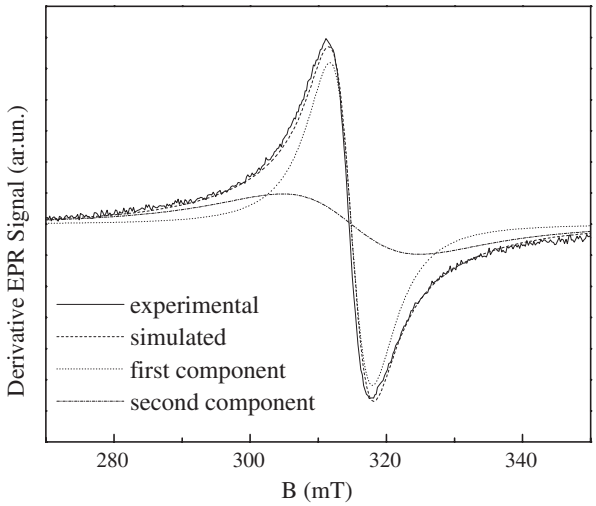

Figure 8. EPR signal of the Mn doped sample as resolved in two components of different ΔB.

4. Discussion and conclusions

The EPR signal of the $CaCu_3Ti_4O_{12}$ powder samples observed in [9], symmetric down to very low temperatures, was interpreted as being due to the average, along the three main directions, of the signals of Cu^{2+} in square-planar oxygen coordination. In addition, no magnetic transition was evident and an asymmetric signal was observed at 4.2 K. The temperature behaviour of the signal intensity was not described.

We will re-propose a CF approach in order to make clear the level structure of a Cu^{2+} ion ($3d^9$: $L = 2$, $S = 1/2$) in a square-planar oxygen coordination by starting, *ab initio*, from the positions of the surrounding ions. We calculated the electrostatic potential $V(r)$ due to the charges q_j at the positions R_j according to the expression $V(r) = \sum_j q_j/4\pi\varepsilon_0|(R_j - r)|V(r)$ which was expanded in tesseral harmonics, sin (s) and cos (c) type, using the Legendre polynomials. Finally, we obtained the expression of the Hamiltonian H_{CF} in terms of the Stevens equivalent operators:

$$H_{CF} = \sum_{nm} F_{nm}^{c/s} O_{nm}^{c/s} \qquad \text{with } F_{nm}^{c/s} = -|e|\langle r^n\rangle a_{nm}^{c/s} c_{nm}^{c/s} \vartheta_n,$$

where $c_{nm}^{c/s}$ have been calculated as a function of the anionic coordinates, $a_{nm}^{c/s}$ are suitable numerical factors, ϑ_n are the Stevens multiplicative factors and $\langle r^n\rangle$ is the expectation value of r^n for the d-orbitals of the Cu^{2+} ion [12]. The Cu^{2+} ion eigenstates and eigenvalues have been calculated by diagonalizing the 10×10 matrix obtained from the Hamiltonian

$$H = H_{CF} + H_{SO} = -|e|V(r) + \lambda \boldsymbol{L} \cdot \boldsymbol{S}$$

operating in the basis $|L, M_L, S, M_S\rangle$. Then, in order to obtain the g-tensor and, more generally, the EPR response, the Zeeman Hamiltonian $H_Z = \mu_B(\boldsymbol{L} + 2\boldsymbol{S}) \cdot \boldsymbol{B}$ is applied on the low-lying energy levels; the g-values are obtained from the resonance condition

$$h\nu = g\mu_B B = \langle\psi_a|H_Z|\psi_a\rangle - \langle\psi_b|H_Z|\psi_b\rangle$$

between the ψ_a and ψ_b states which diagonalize H_Z.

For a square-planar coordination and $\lambda = 0$, the following orbital level distribution is obtained:

(a)	(b)
$3z^2 - r^2$	$3z^2 - r^2$
xz, yz	xz, yz
$x^2 - y^2$	xy
xy	$x^2 - y^2$

where (a) refers to x, y axes parallel to the square sides (more suitable if a not perfectly square-planar coordination (e.g. rectangular coordination) is considered) and (b) refers to x, y axes parallel to the square diagonals.

In the two cases $g_x = g_y = g_z = 2$.

By assuming $\lambda \neq 0$, the spin–orbit interaction couples the xy and $x^2 - y^2$ states (split by Δ) and these in turn with the xz, yz states (split by Δ_1), so the ground state results in the spin doublet:

$$\psi_a = a|xy, 1/2\rangle + b|(x^2 - y^2), 1/2\rangle + c|-1, -1/2\rangle$$
$$\psi_b = a|xy, -1/2\rangle + b|(x^2 - y^2), -1/2\rangle + c|1, 1/2\rangle$$

with $a > b$ (case a), $a < b$ (case b) and $c \ll a, b$.

The $\langle\psi_a|H_Z|\psi_a\rangle$ and $\langle\psi_b|H_Z|\psi_b\rangle$ matrix elements of H_Z are different in the x and y directions with respect to the z-direction and $g_z > g_x = g_y = 2$.

In more detail, for $\lambda = -710$ cm^{-1} [13] and $\Delta \cong 12\,000$ cm^{-1} [14], $g_z \cong 4$ and $g_x = g_y = 2$ are obtained. This result disagrees with the experimental data, in that the EPR signal is really isotropic in the temperature range 25–500 K, so, in a simple CF approach, we must suppose that $\lambda/\Delta \to 0$. Nearly the same results are obtained by considering also the second and third oxygen square-planar coordinations.

For completeness, we report here the Cu^{2+} ground spin doublet in a regular dodecahedral coordination (ideal perovskite):

$$\psi_a = a|xy, 1/2\rangle + c|-1, -1/2\rangle \qquad \psi_b = a|xy, -1/2\rangle - c|1, 1/2\rangle \qquad \text{(case a)}$$

or

$$\psi_a = a|(x^2 - y^2), 1/2\rangle + c|-1, -1/2\rangle \qquad \psi_b = a|(x^2 - y^2), -1/2\rangle - c|1, 1/2\rangle. \qquad \text{(case b)}$$

The resulting g-factor is isotropic and equal to 2 for any λ-value $\neq 0$.

The ground state is an orbital singlet for symmetry reasons in the square-planar coordination, or *via* spin–orbit coupling, as in the regular dodecahedron, so there is no need to invoke the Jahn–Teller (JT) effect [6] to remove the orbital level degeneration. The g-value and the line-shape could be appropriate to a Cu^{2+} signal from the dynamic JT effect [13]; degenerate orbital ground states with mean g-values consistent with the experimental one could be obtained, but from not realistic tetragonal distortions of the dodecahedron. Indeed, the structural data assign to Cu^{2+} ions an effective square-planar coordination, so a highly asymmetric EPR signal is expected for polycrystalline samples. Besides, due to the very small EPR line-width, a symmetric signal should result from the average of asymmetric signals along the three main directions only if $g_\parallel$ and $g_\perp$ differ of some per cent. As consequence a simple CF approach is inadequate.

Rather, the observed isotropic EPR signal with $g = 2.15$ can be justified by a strong delocalization of the copper-hole on the four next neighbouring oxygen ions, in agreement

with the already asserted strong covalent character of the Cu–O bond [15]. Each oxygen ion of the Cu square-planar coordination is shared with an octahedron of the Ti coordination, so that the copper-hole delocalization allows an AF super-exchange interaction, *via* Ti d-orbitals, along the (111) direction. This interaction ($J_3 = 2\ \mathrm{cm}^{-1}$) is invoked to justify the AF ordering at T_N as due to the AF coupling between two F-coupled Cu sublattices lying in planes normal to the (111) direction [16], even if no agreement exists in the literature about the relative intensity of these interactions [8].

Regarding the EPR line-width, the anomalous temperature behaviour, showing a minimum at about 235 K, could be related to the presence of a disordered state at low temperature and a more ordered state at high temperature with a crossover temperature in the 200–300 K range [15].

Finally, the weaker component of the EPR signal with constant resonant field ($g = 2.15$) for $T < T_N$ and $I_4/I_{25} = 1/60$ for the pure-a sample can be ascribed to the paramagnetic centres not contributing to the magnetic order because of their boundary location. On considering the linear dimension ($\sim$0.74 nm) of the unit cell, the ratio between the number of boundary and internal ions is 1/60 if the grain dimension is about 0.3 μm, as is indeed obtained from FWHM measurements of XRPD peaks. At 4 K this signal component, the only one observed, is symmetric, contrary to what was reported by [9], and so excludes Cu–O bond ionic strength enhancement with decreasing temperature [16].

Whereas the EPR signal of the sample with substitution in Ca sites is practically the same as that of the pure-a sample, the EPR signals of the samples with substitution in Ti sites, resulting from the superposition of signals with the same g-factor but different ΔB values, show the important role of the Ti site [17] on the magnetic interactions: sample regions are formed, giving rise to the same EPR signal but with larger line-width and showing no AF transition. The enhancement of dipolar interactions, due to the presence of non-null magnetic moments instead of the Ti^{4+} null magnetic moment, and the reduction of the exchange narrowing, due to the interactions between dissimilar ions, can be responsible for the signal broadening. The hindering of the magnetic transition, evidenced by the increase (related to the I_4/I_{25} value) of the paramagnetic signal component with constant resonant field for $T < 25$ K, can be ascribed to the presence of non-empty d-orbitals on the Ti site, which could forbid the whole AF double super-exchange interaction at 90° along the (111) direction.

As already observed [2], the dielectric properties are also strongly affected by substitutions on the octahedral Ti sites, whereas much weaker effects are noticed with substitutions on the dodecahedral Ca site.

Interesting features arise concerning the pure-b sample with about 0.5% of Cu vacancies. The dramatic reduction of the signal intensity with respect to the pure-a sample suggests that Cu^{2+} ions cannot be merely considered directly responsible for the EPR signal. Such a huge intensity decrease cannot be explained even by supposing the presence of Cu^{3+} in square-planar coordination, which is not EPR active [18]. Also, in the pure-b sample, a paramagnetic phase exists for $T < T_N$ with the I_4/I_{25} value very much higher than that for the pure-a sample; the extent of the paramagnetic phase can be only partially attributed to the small increase of non-magnetically correlated Cu ions. We outline also that, for samples with Cu^{2+} vacancies, a strong reduction of the dielectric constant has been observed [2].

In conclusion, this work should encourage new suggestions for the interpretation of the not yet wholly explained properties of $CaCu_3Ti_4O_{12}$. Nevertheless, we can state that a simple crystal-field approach is not suitable to interpret the EPR signal and further models should be deepened to justify the EPR response, taking the Cu-hole delocalization also into account. In addition, from the results obtained with substitutions on Ti and Ca sites, we can outline that the CuO_4–TiO_6–CuO_4 complexes are strongly interconnected and that also small

variations of their configuration give rise to very important changes in the magnetic and EPR features.

References

[1] Ramirez A P, Subramanian M A, Gardella M, Blumberg G, Li D, Vogt T and Shapiro M S 2000 *Solid State Commun.* **115** 217
[2] Subramanian M A, Li D, Duan N, Reisner B A and Sleight A W 2000 *J. Solid State Chem.* **151** 323
[3] Subramanian M A and Sleight A W 2002 *Solid State Sci.* **4** 347
[4] Sinclair D C, Adams T B, Morrison F D and West A R 2002 *Appl. Phys. Lett.* **80** 2153
[5] Bochu B, Deschizeauix M N, Joubert J C, Collomb A, Chenavas J and Marezio M 1979 *J. Solid State Chem.* **29** 291
[6] Moussa S M and Kennedy B J 2001 *Mater. Res. Bull.* **36** 2525
[7] Collomb A, Samaras D, Bochu B and Joubert J C 1977 *Phys. Status Solidi* a **41** 459
[8] Kim Y J, Wakimoto S, Shapiro S M, Gehring P M and Ramirez A P 2002 *Solid State Commun.* **121** 625
[9] Propach V 1977 *Inorg. Allg. Chem.* **435** 161
[10] Rodriguez-Carvajal J 1993 *Physica* B **192** 55
[11] Massarotti V, Capsoni D, Bini M, Azzoni C B and Paleari A 1997 *J. Solid State Chem.* **128** 80
[12] Hutchings M T 1964 *Solid State Physics* vol 16 (London: Academic) pp 227–73
[13] Abragam A and Bleaney B 1970 *Electron Paramagnetic Resonance of Transition Ions* (Oxford: Clarendon) chapter 7
[14] Homes C C, Vogt T, Shapiro S M, Wakimoto S, Subramanian M A and Ramirez A P 2003 *Phys. Rev.* B **67** 0092106
[15] Božin E S, Petkov V, Barnes P W, Woodward P M, Vogt T, Mahanti S D and Billinge S J L 2003 *Preprint* cond-mat/0303189 v1
[16] Koitzsch A, Blumberg G, Gozar A, Dennis B, Ramirez A P, Trebst S and Wakimoto S 2002 *Phys. Rev.* B **65** 052406
[17] Johannes M D, Pickett W E and Weht R 2002 *Matter. Res. Soc. Symp. Proc.* **718** 25
[18] Azzoni C B and Paleari A 1994 *J. Phys.: Condens. Matter* **6** 4699